Eur Biophys J (2010) 39:1079–1088
DOI 10.1007/s00249-009-0504-3

ORIGINAL PAPER

# Stochastic simulation of calcium microdomains in the vicinity of an L-type calcium channel

**Frederic von Wegner · R. H. A. Fink**

Received: 22 February 2009 / Revised: 29 May 2009 / Accepted: 8 June 2009 / Published online: 1 July 2009


**Abstract** We study numerically the local dynamics of the intracellular calcium concentration in the vicinity of a voltage- and calcium-dependent plasma membrane L-type calcium channel. To account for the low number of $Ca^{2+}$ ions and buffer molecules present in sub-femtoliter volumes, we use an exact stochastic simulation algorithm including diffusion. We present a novel, unified simulation method that implements reaction-diffusion events of $Ca^{2+}$ ions and buffer molecules, stochastic ion channel gating and channel conductance as a multivariate Markov process. For fixed-voltage dynamics, e.g. under voltage-clamp conditions, it is shown that voltage-sensitive channel-gating steps can be incorporated exactly. We compare multi- and single-voxel geometries and show that the single-voxel approach leads to almost identical first- and second-order moments, at much lower computation time. Numerical examples illustrate the variability in local $Ca^{2+}$ fluctuations as induced by bursts of channel openings in response to membrane depolarisations. Finally, by introducing calmodulin as a link, it is shown how this variability is passed on to downstream signalling pathways. The method may prove useful to study calcium microdomains and calcium-regulated processes triggered by membrane depolarisations as evoked by, e.g., viral channel-forming proteins during virus-host cell interactions.

**Keywords** Multivoxel stochastic simulation · Calcium · Microdomains · Calcium channels

Viral membrane proteins, Heidelberg, December 2008.

F. von Wegner (✉) · R. H. A. Fink
Medical Biophysics, Institute for Physiology and Pathophysiology, University of Heidelberg, INF 326, 69120 Heidelberg, Germany
e-mail: fwegner@physiologie.uni-heidelberg.de

## Introduction

The dynamics of subcellular, localised calcium fluctuations is governed by stochastic events comprising buffer association and dissociation reactions, diffusion events and transitions between functional states of larger protein molecules such as enzymes and ion channels, the latter often viewed as jumps between quasi-discrete states. Free calcium ions ($Ca^{2+}$) play a special role in intracellular signal transduction as elevations of the usually low intracellular resting calcium concentration ($[Ca^{2+}]_i \sim 100$ nM) regulate numerous calcium-sensitive proteins (e.g. calmodulin—CaM, protein kinase A, calcineurin) that participate in a large number of cell-type-specific second-messenger pathways (e.g. CaM-kinase, MAP-kinase, diacylglycerol) regulating cellular motility, gene transcription, membrane excitability or vesicle fusion (Cheng and Lederer 2008). This diversity in biological function contrasts with the simple chemical structure of $Ca^{2+}$ ions and the clearly defined physical and chemical properties of $Ca^{2+}$ ions provide a favourable stating point for mathematical models and numerical simulations.

In this report, we focus on the formation of $Ca^{2+}$ microdomains in the vicinity of a plasma membrane that contains L-type calcium channels (LCC) as well as diffusible and immobile buffer molecules, using stochastic numerical algorithms. L-type calcium channels are voltage- and calcium-sensitive proteins that form a larger family of variants and which can be found in various cell types such as skeletal and cardiac muscle and neurons but also in many non-excitable cells in humans and other vertebrates (Catterall et al. 2005). Due to extensive electrophysiological investigations, kinetic properties of many L-type calcium channels are now known in different expression systems (Catterall et al. 2005). Also, the

existence of spontaneous, localised $Ca^{2+}$ elevations (e.g. $Ca^{2+}$ 'sparks') and their action on nearby $Ca^{2+}$-sensitive subcellular structures ($K^+$ channels, mitochondria) have been shown using high-resolution dynamic fluorescence microscopy (Demuro and Parker 2004; Cheng and Lederer 2008). Within these calcium microdomains, local feedback and temporal correlations between the calcium concentration and ion channel kinetics occur due to calcium buffers with different kinetics and the calcium sensitivity of calcium channels, e.g. LCC. The typical length scale of these microdomains is approximately 100–1,000 nm, which is the scale of cellular organelles, macromolecular assemblies (ion channel clusters, vesicles) and calcium microdomains (Cheng and Lederer 2008), and at the same time, can be observed by current state-of-the-art microscopy techniques. It is important to realise that in the context of calcium signalling, at the upper end of the considered scale, a $(1{,}000\ \text{nm})^3 = 1$ fl volume contains as little as 60 $Ca^{2+}$ ions (100 nM) on average. Moreover, even a single LCC can contribute significantly to the dynamics of a local calcium microdomain (Demuro and Parker 2004).

In numerical simulations of cell types such as skeletal and cardiac muscle where depolarisations lead to large calcium currents via intracellular calcium-release channels, this problem is frequently solved by a mixed computational approach, using a deterministic method for calcium dynamics and a stochastic algorithm to simulate ion channel gating (Stern et al. 1997, 1999; Hinch et al. 2004; Greenstein and Winslow 2002; Rüdiger et al. 2007). In a similar approach, these methods have recently been used to study the influence of buffers on the gating of small numbers of intracellular 1,4,5-inositol-trisphosphate ($IP_3$) $Ca^{2+}$-release channels (Shuai et al. 2007, 2008). Numerical simulations of calcium microdomains (e.g. $Ca^{2+}$ 'sparks') that do not model channels explicitly are usually completely deterministic, partial differential equation (PDE)-based models (Smith et al. 1998; Jiang et al. 1999; Uttenweiler et al. 2002). In these models, the resting $Ca^{2+}$ concentration appears as a constant value, ignoring the intrinsic stochasticity due to buffering and diffusion.

Using a simplified model of calcium buffering, Bhalla addressed this problem in a computational model of a neuronal synapse, modelling equilibrium $[Ca^{2+}]$ stochastically as a single first-order reaction (Bhalla 2004). Winslow and co-workers proposed a detailed model of the cardiac dyad using a stochastic algorithm based on the Fokker–Planck equation (Winslow et al. 2006) where $Ca^{2+}$ buffering and diffusion are treated stochastically. A recent, detailed Brownian dynamics simulation of $Ca^{2+}$-dependent signalling in a neuronal synapse focusing on calmodulin activation can be found in Keller et al. (2008). In the latter model, all particles are treated individually, giving the most detailed picture. Here, $Ca^{2+}$ dynamics is treated on a mesoscopic level, i.e. the algorithm tracks the total number of ions and buffer molecules rather than the three-dimensional path of each individual reactant.

Here, we present a unified, purely stochastic framework to simulate all participating processes as a multivariate Markov process based on Gillespie's exact stochastic algorithm with diffusion (Gillespie 1977; Elf et al. 2003), extended to include the voltage- and calcium-dependent kinetics of LCC gating as well as a simplified model of $Ca^{2+}$ permeation through the channel pore.

The present study was motivated by recent findings considering the role of altered membrane conductances during membrane fusion and replication of pathogenic viruses. Viral proteins themselves can form cation channels ($Na^+$, $K^+$, $Ca^{2+}$). These cation-selective ion channels can lead to an increase in intracellular $[Ca^{2+}]$ via their intrinsic $Ca^{2+}$ conductance or by membrane depolarisation and subsequent activation of host-cell voltage-gated calcium channels, e.g. LCC, a possible mechanim by which $Ca^{2+}$ channel blockers inhibit viral infection (Griffin et al. 2003; Frohns et al. 2006; Lu et al. 2006). The detailed structure of some of these viral proteins is known, and molecular dynamics (MD) simulations have been employed to clarify structure–function relationships (Fischer and Sansom 2002; Fischer 2005). Increased $[Ca^{2+}]$ seems to be directly involved in the intracellular pathways responsible for virus replication (Bouchard et al. 2001). These subcellular processes occur in the microdomain as discussed above. The method proposed in the present work may help to bridge the gap in temporal and spatial scales between atomic-scale (MD) and whole-cell simulations. The increasing knowledge about the kinetics of these viral proteins can be readily incorporated in the presented theoretical framework to study the inherently stochastic dynamics of virus–host interactions on a subcellular scale quantitatively. Finally, the method can easily be applied to any model system for which sufficient biophysical data are at hand (e.g. skeletal and cardiac muscle, neurons).

## Simulation of chemical reactions

### Gillespie's algorithm

Numerical simulations were carried out using an extension of Gillespie's algorithm for the exact stochastic simulation of a set of chemical reactions (Gillespie 1977). In Gillespie's algorithm, macroscopic reaction rate constants are transformed into waiting-time distributions and thus, into time- and state-dependent probabilities. This procedure can be carried out for each process for which a rate constant is available, e.g. also for diffusion events (see below). Similarly, transitions between functional states of channel

proteins are usually also modelled as a jump Markov process where each state corresponds to a set of functionally equivalent protein conformations (Smith 2002). Transition rates between these states, from which stochastic waiting-time distributions are calculated, can be measured experimentally using e.g. voltage-clamp protocols. Finally, ion permeation through a channel pore is also a stochastic process introducing another source of variability (Kuyucak et al. 2001; Krishnamurty and Chung 2007)—here, we use the average channel conductance to compute a stochastic permeation rate constant. In summary, the term reaction is to be interpreted in a general sense, including:

- Chemical reactions: association and dissociation reactions of $Ca^{2+}$ ions and buffer molecules, also $Ca^{2+}$ binding to the channel
- Diffusion events
- Channel gating: jumps between discrete ion-channel states
- Channel conductance: permeation of $Ca^{2+}$ ions through the channel pore

We here give a brief summary of the classic Gillespie algorithm (Gillespie 1977). The state vector $\mathrm{x}(t) = (\mathrm{x}_1(t), \ldots, \mathrm{x}_N(t))$ denotes the number of each reactant $\mathrm{x}_k, k = 1, \ldots, N$ present in the simulation volume at time $t$, including the set of discrete channel states. Each of the $M$ reactions $R_j, j = 1, \ldots, M$ that can occur in the system has a reaction propensity $a_j(\mathrm{x},t) = c_j \times h_j(\mathrm{x},t)$, where $c_j$ is a volume-adapted, stochastic rate constant and $h_j(\mathrm{x},t)$ denotes the number of possible molecular combinations available for reaction $R_j$ at time $t$. For the mono- and bimolecular reactions in the present model, the stochastic rate constants $c_j$ are calculated from the macroscopic reaction rate constants $k_j$ as $c_j = k_j$ for monomolecular reactions and as $c_j = k_j/V$ for bimolecular reactions given the single-voxel volume $V$.

A random waiting time $\tau$ is computed for each reaction and stored in a waiting-time queue. The waiting time for a chemical reaction is computed from the current reaction propensity and a uniformly distributed random variable $r \sim \mathrm{U}_{[0,1]}$ (Press et al. 2002) as:

$$\tau = -\ln(r)/a_j(\mathrm{x},t) \tag{1}$$

Equation 1 leads to exponentially distributed waiting-time distributions characteristic of Markovian systems. In the next step, the system state is updated according to the stoichiometric coefficients of the reaction with the lowest waiting time. The current simulation time $t$ is advanced by $t \leftarrow t + \tau$ and the procedure enters the next iteration. Computational efficiency is achieved by updating only those reaction rates and waiting times that are affected by the current reaction (Gibson and Bruck 2000). Dependencies between molecular species and reactions are stored in a dependency graph as introduced by Gibson and Bruck (2000).

## Multivoxel simulation and diffusion

In the classic Gillespie algorithm, a single reaction volume is considered. To introduce spatial resolution and to account for diffusion effects, the volume of interest, $V_0$, is decomposed in a set of $n_\mathrm{V}$ sub-voxels of volume $V = V_0/n_\mathrm{V}$. The above described sampling of waiting times for the class of chemical reactions has to be computed for each voxel. Diffusion is introduced using a stochastic diffusion rate constant $d_{ik} = D_i \big/ (\Delta \mathrm{x})^2$, $i = 1, \ldots, N$, $k = 1, \ldots, n_\mathrm{V}$ assigned to each reactant particle (index $i$) and each voxel (index $k$) as detailed by Elf and colleagues (Elf et al. 2003). The diffusion rate depends on the macroscopic diffusion coefficient $D_i$ and the voxel volume $V = (\Delta x)^3$. For each reactant (index $i$) and each voxel (index $k$), a random waiting time is generated according to:

$$\tau = -\ln(r)/d_{ik} \tag{2}$$

where $r$, again, is a uniformly distributed random variable ($r \sim \mathrm{U}_{[0,1]}$). Thus, diffusion events also follow an exponential waiting-time distribution and easily integrate into the Markovian framework.

We now describe the details of the reactions and processes of the model used in the present work.

## Calcium buffering

Calcium ions participate in a number of buffering reactions with mobile and immobile molecules and can be bound to and dissociate from the calcium channel. Due to reversibility, these reactions always occur in pairs, a bimolecular association reaction:

$$\mathrm{Ca}^{2+} + \mathrm{B} \rightarrow \mathrm{CaB} \tag{3a}$$

and a monomolecular dissociation reaction:

$$\mathrm{CaB} \rightarrow \mathrm{Ca}^{2+} + \mathrm{B}. \tag{3b}$$

The kinetics of each of these reactions is given by the rate constants $k_j^+$ and $k_j^-$ for association and dissociation reactions, respectively. Numerical values are summarised in Table 1.

## Simulation of the L-type calcium channel (LCC)

We consider the LCC model proposed by Jafri and colleagues (Jafri et al. 1998; Greenstein and Winslow 2002), based on experimental data in cardiac myocytes. The gating scheme is illustrated in Fig. 1a. The LCC is modelled as a tetramer with four independent subunits where each

**Table 1** Kinetic constants and diffusion coefficients

| Reactant | $k^+$ ($\mu M^{-1}$ $ms^{-1}$) | $k^-$ ($ms^{-1}$) | $K_D$ ($\mu M$) | D ($\mu m^2$ $s^{-1}$) | $B_T$ ($\mu M$) | References |
|---|---|---|---|---|---|---|
| $Ca^{2+}$ | | | | 200 | – | |
| B1 | 0.1 | 0.1 | 1.0 | 100 | 100 | – |
| B2 | 0.01 | 0.01 | 1.0 | 100 | 100 | – |
| B3 | 0.001 | 0.001 | 1.0 | 100 | 100 | – |
| Fluo-4 | 0.234 | 0.175 | 0.7479 | 100 | 50 | Uttenweiler et al. 2002 |
| CaM | 0.1 | 0.038 | 0.38 | 0 | 24 | Smith et al. 1998 |
| SL | 0.115 | 1 | 8.696 | 0 | 1,124 | Smith et al. 1998 |

subunit has two functional states, open and closed. The channel is in the open state when all four subunits are in the open conformation. In each of the five closed states (Fig. 1a, $C_0$–$C_4$), the tetramer can bind a $Ca^{2+}$ ion. The set of calcium-bound states is termed the calcium mode whereas the non-calcium-bound states are termed normal mode (Jafri et al. 1998). The channel can switch to the $Ca^{2+}$-conducting open state from both modes (normal mode $C_4 \leftrightarrow O$, calcium mode $C'_4 \leftrightarrow O_{Ca}$, Fig. 1a).

The single subunit transitions between closed and open conformations are voltage-dependent, and the rate constant follows the general law:

$$\alpha = \alpha_0 \times \exp(\alpha_1 \times (V_m - V_0)) \tag{4a}$$

$$\beta = \beta_0 \times \exp(\beta_1 \times (V_m - V_0)) \tag{4b}$$

Mode transitions between any (normal mode) closed-state C and the corresponding (calcium mode) state C′ are modelled as a buffering reaction:

$$Ca^{2+} + C \rightarrow C' \tag{5a}$$

$$C' \rightarrow Ca^{2+} + C. \tag{5b}$$

Open-closed state transitions ($C_4 \leftrightarrow O$, $C'_4 \leftrightarrow O_{Ca}$) have fixed transition rates.

Whereas $Ca^{2+}$-dependent mode transitions are easily integrated in the framework of chemical reactions, voltage-dependent reaction rates change continuously through time. This violates one of the assumptions implicitly used when applying Gillespie's algorithm, i.e. that all reaction rates are constant between individual events; as a consequence, in the Gillespie algorithm, time is advanced until the first reaction time is encountered and rates have to be updated. Here, we have to include the more general formula for the waiting time of a Markov process with a continuously time-varying rate $a_j(x,t)$, which is derived from the differential evolution equation of the Markov chain (Norris 1997):

$$p(\tau|x,t) = \exp\left(-\int_t^\tau a_j(x,s)ds\right) \tag{6a}$$

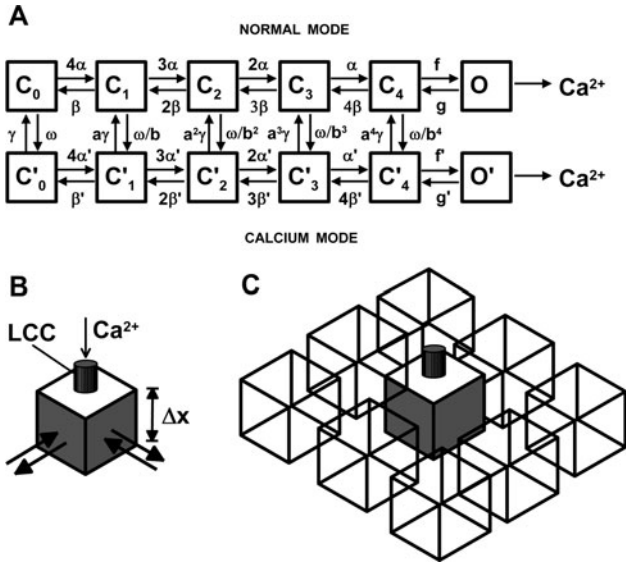


**Fig. 1a, b** Simulation scheme. **a** Gating scheme of the cardiac L-type calcium channel as proposed in Jafri et al. (1998) and Greenstein and Winslow (2002). The channel is modelled as a tetramer that is open when all four subunits are in the open state, i.e. there are five closed states and one open state in each mode. The two modes ('normal' and 'calcium') indicate whether a $Ca^{2+}$ ion is bound to the channel or not. **b** In the single-voxel algorithm, the reaction volume is a cube that exchanges mobile reactants with a 'constant pool' outside the cube where all reactant concentrations are held constant. Additional $Ca^{2+}$ ions can enter the simulation volume via a single L-type calcium channel (LCC, *arrow*). **c** In the multivoxel approach, a cubic array of simulation volumes is created. Reactant exchange occurs by diffusion and only the central voxel contains the LCC. A constant pool is assumed as a boundary condition

which is implemented using the transformation method (Press et al. 2002):

$$\int_t^\tau a_j(x,s)ds = \xi = -\ln(r) \tag{6b}$$

Equation 6b is interpreted in the following way: first, an exponentially distributed random variable $\xi$ is generated from a uniformly distributed random variable $r$. In a second step, the non-negative reaction rate $a_j(x,t)$ is integrated until the integrated value "hits" $\xi$. A short calculation

verifies that in the case of a constant rate $a_j(x,t)$, the above formula is equivalent to the Gillespie algorithm. In our case, as voltage is assumed to be under the control of the experimenter, the voltage time course is known in advance and the waiting time can be calculated analytically. In the numerical experiments presented below, sample paths of 100-ms duration are generated and a depolarisation from −70 to +20 mV is introduced for 50 ms (25–75 ms). This leads to a piecewise linear shape of the time-integrated rates $\alpha$, $\alpha'$, $\beta$, $\beta'$ that is easily inverted analytically. After each voltage-sensitive state transition, a new random waiting time is generated according to Eq. 6b and introduced in the waiting-time queue.

The calcium channel itself acts as a calcium source, i.e. the channel generates 'conductance events' that introduce $Ca^{2+}$ ions into the system, thereby disturbing the chemical equilibrium. A conductance event can occur when the channel occupies one of the two open states; in the reaction scheme, the channel occurs on both sides as it is not changed under the event:

$$O \rightarrow O + Ca^{2+} \tag{7a}$$

$$O_{Ca} \rightarrow O_{Ca} + Ca^{2+}. \tag{7b}$$

The channel current $i_{Ca}$ is voltage-dependent (Jafri et al. 1998), and therefore, a $Ca^{2+}$ permeation rate $\rho$ exists for each transmembrane voltage, $\rho = (i_{Ca} \times N_A)/(2 \times F)$, where $F$ and $N_A$ denote Faraday's and Avogadro's constants, respectively. This implementation leads to a Poisson model of $Ca^{2+}$ release, i.e. the number of released $Ca^{2+}$ ions follows a Poisson distribution, and the waiting times between single conductance events are exponentially distributed. Although a Poisson model may be too simple given the results obtained with molecular dynamics simulations (Kuyucak et al. 2001), on a sub-femtoliter scale, a stochastic $Ca^{2+}$ release model appears to be a more realistic assumption than a constant current model (Keller et al. 2008).

LCC parameters used are identical to the values given by Greenstein and Winslow (2002): $f = 0.85\ s^{-1}, g = 2.0\ s^{-1}$, $f' = 0.005\ s^{-1}$, $g' = 7.0\ s^{-1}$, $a = 2.0$, $b = 1.9356$, $\gamma_0 = 0.44\ mM^{-1}\ ms^{-1}, \omega = 0.02158\ ms^{-1}, \alpha_0 = 2.0, \alpha_1 = 0.012$, $\beta_0 = 0.0882$, $\beta_1 = -0.05$, $\alpha' = \alpha \times a$, $\beta' = \beta/b$, $\gamma = \gamma_0 \times [Ca^{2+}]_0$, $V_0 = 35$ mV.

### Geometry

Two geometries are considered—single- and multivoxel cubes. Both are illustrated schematically in Fig. 1b, c. As explained above, the LCC current disturbs the local chemical equilibrium, and therefore, diffusion has to be incorporated in the model. A spatially resolved multivoxel extension of the Gillespie algorithm was introduced a few years ago by Elf and colleagues (Elf et al. 2003). As the multivoxel algorithm is computationally more expensive and since we are mainly interested in the local $Ca^{2+}$ dynamics in the vicinity of the LCC, we designed a single-voxel algorithm with diffusion. The single voxel contains the LCC and exchanges diffusible reactants with a 'constant pool' where all diffusion rates (i.e. concentrations) are held constant (Fig. 1b). The same technique is applied in the periphery of the multivoxel algorithm. In the multivoxel geometry, the LCC is put in the central voxel of one of the sides of the simulation cube, representing the plasma membrane (Fig. 1c). Moreover, diffusion is modelled with a reflecting boundary on the side of the plasma membrane. We consider sub-femtoliter voxel volumes; detailed values are given in the "Results" section.

### Computations

Algorithms were implemented in C++ and run on a PC (Pentium4 DualCore, GHz, 2GB RAM).

## Results

### Calcium fluctuations at equilibrium

Intrinsic stochastic fluctuations of the microdomain $Ca^{2+}$ concentration at equilibrium are illustrated in Fig. 2, where sample paths of the free $Ca^{2+}$ concentration obtained with the single-voxel algorithm at different volumes are shown. To quantify equilibrium fluctuations, simulations were carried out in a simplified model without calcium channels in the presence of three model buffers (B1-3: $k_1^+ = 0.1\ \mu M^{-1} ms^{-1}$, $k_1^- = 0.1\ ms^{-1}$, $k_2^+ = 0.01\ \mu M^{-1} ms^{-1}$, $k_2^- = 0.01\ ms^{-1}$, $k_3^+ = 0.001\ \mu M^{-1} ms^{-1}$, $k_3^- = 0.001\ ms^{-1}$, total buffer concentration $B_1^T = B_2^T = B_3^T = 100\ \mu M$, diffusion coefficients $D_{1-3} = 100\ \mu m^2\ s^{-1}$). This mixture of buffers with kinetic rate constants spanning three orders of magnitude was designed to reflect the intracellular milieu in many cell types. Specific intracellular buffers and their measured kinetics are introduced further below.

Simulation results are shown for a mean $[Ca^{2+}]$ of 100 nM and the following volumes: $(250\ nm)^3 = 0.015625$ fl (upper row), $(500\ nm)^3 = 0.125$ fl (middle row), and $(1{,}000\ nm)^3 = 1$ fl (lower row). The left column contains 100-ms sample paths of the free $Ca^{2+}$ concentration using a sampling rate of 100 kHz. To the right of each $Ca^{2+}$ time course, the corresponding time-averaged $[Ca^{2+}]$ distribution after linear interpolation of the sample path is shown. Distributions at small volumes are highly skewed, whereas for 1 fl, the distribution is symmetric and is well approximated by a Gaussian curve (not shown). Also, the dispersion of the distribution is higher for small volumes—

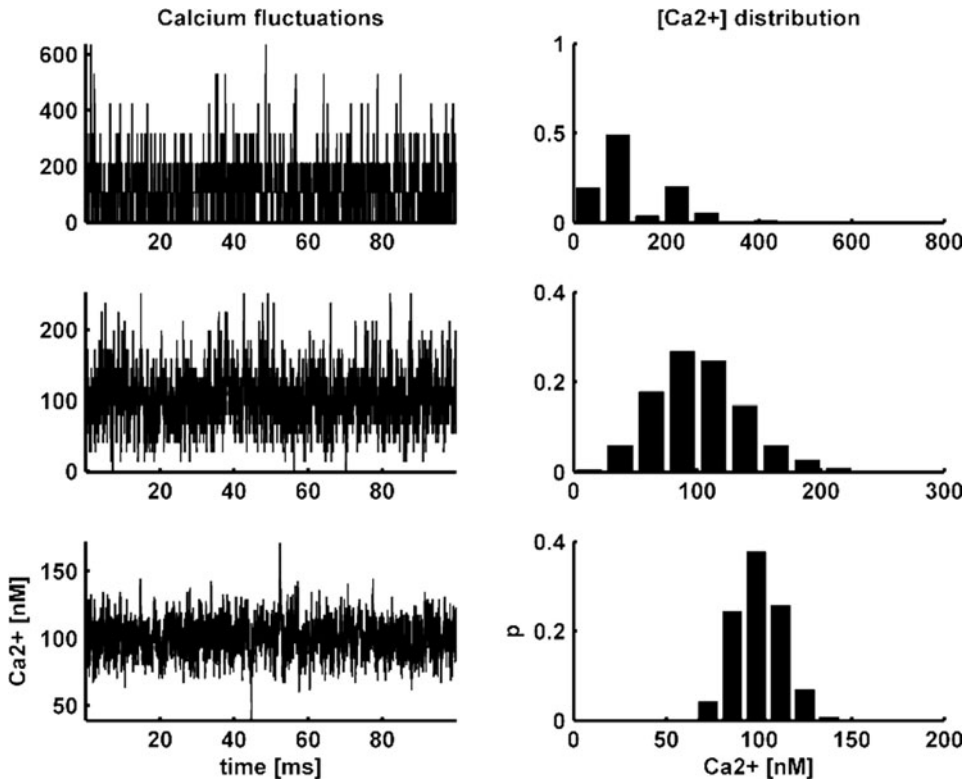


**Fig. 2** Equilibrium fluctuations. The equilibrium distribution for 100 nM of free $Ca^{2+}$ ions in the presence of buffers $B_1$–$B_3$ is simulated for different volumes using the single-voxel algorithm. Simulation volumes are $(250\ \text{nm})^3 = 0.015625$ fl (*upper row*), $(500\ \text{nm})^3 = 0.125$ fl (*middle row*) and $(1{,}000\ \text{nm})^3 = 1$ fl (*lower row*). The sample paths (100 ms) in the *left column* show the calculated $Ca^{2+}$ concentration using a sampling rate of 100 kHz. In the *right column*, the correponding time-averaged [$Ca^{2+}$] histograms after linear interpolation of the sample path on the left are shown. Distributions at small volumes are highly skewed, whereas for 1 fl, the distribution is symmetric and can be approximated by a Gaussian curve (not shown). The coefficients of variation for the different conditions are approximately (*from the top*) 0.74 (128 ± 95 nM), 0.38 (102 ± 38 nM) and 0.13 (99 ± 13 nM)

for increasing volumes, the coefficients of variation are approximately 0.74 (128 ± 95 nM), 0.38 (102 ± 38 nM) and 0.13 (99 ± 13 nM), as derived from $n = 10$ simulation runs. It is seen that for sub-femtoliter volumes, and even in the absence of a calcium channel, significant fluctuations of the local $Ca^{2+}$ concentration should be expected.

## Single- and multivoxel geometries

Before the calcium channel is introduced in the model, we will quantify the effects of diffusion and the choice of geometry on statistical properties of calcium fluctuations. The different algorithms discussed above (classic Gillespie, multivoxel with diffusion, single-voxel with diffusion) should give consistent results. This cannot be expected a priori as diffusion events by far outnumber chemical reaction events and therefore represent another source of variability. Furthermore, comparing the single- and multivoxel algorithms is necessary to evaluate effects of the constant pool assumption as an approximated boundary condition. All results are 'recorded' from a 1-fl box.

The reaction system is identical to the system used in Fig. 2, i.e. three calcium buffers with a kinetic range of three orders of magnitude. We used second-order moments to quantify the statistical properties of sample paths. These are best summarised as power spectral densities as shown in the right column of Fig. 3. The autocorrelation time of the sample paths was computed using a first-order autoregressive model and is indicated in the graphs (black diamond).

In Fig. 3a, a sample path obtained with the classic Gillespie algorithm, i.e. a single voxel without diffusion, is shown. Figure 3b corresponds to the single-voxel algorithm with diffusion that we introduced. The simulation in Fig. 3c is obtained from a multivoxel model using 125 voxels ($5 \times 5 \times 5$), with a single-voxel volume of 1 fl. The trace shown corresponds to the $Ca^{2+}$ time course of the central voxel. Finally, Fig. 3d is also based on the multivoxel approach, but the 1-fl volume was divided in 125 subvolumes, i.e. $5 \times 5 \times 5$ cubes of 200-nm length each. The curve represents the number of free $Ca^{2+}$ ions in the whole 1-fl volume. Visual inspection of the sample paths and, more quantitatively, power spectral densities

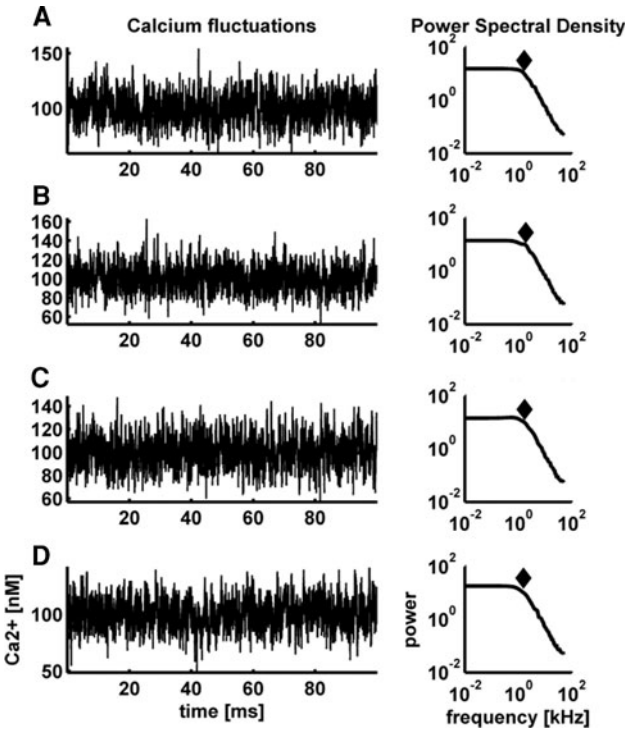


**Fig. 3a–d** Diffusion effects assessed by different simulation methods. **a** Single-voxel method without diffusion or classic Gillespie algorithm, 1 fl. **b** Single-voxel method with diffusion, 1 fl. **c** Multivoxel method, $5 \times 5 \times 5$ 0.008 fl = $(200\ \text{nm})^3$ voxels. **d** Multivoxel method, $5 \times 5 \times 5$ 1-fl voxels. Single simulation runs, sampled at 100 kHz, are shown in the *left column* and corresponding power spectral densities with estimated auto-correlation times (*diamonds*) in the *right column*. All simulations contain 100 nM free $Ca^{2+}$ and three buffers ($B_1$–$B_3$). All methods yield comparable sample paths with almost identical first- and second-order statistics, i.e. mean [$Ca^{2+}$], variance and correlation times

and autocorrelation times show that all approaches are practically equivalent with respect to first- and second-order statistics. Autocorrelation times were approximately 0.09 ms. This effect was also quantified on larger numbers of sample paths (not shown). It should be noted that, even though all algorithms lead to similar statistical properties at equilibrium, in the case that the model contains a calcium channel, a model with diffusion has to be used—otherwise, $Ca^{2+}$ ions would accumulate in the model volume.

## L-type calcium channel

To complete the model, we attach a single L-type calcium channel to the simulation volume. Simulations are all based on the single-voxel method with diffusion. The buffer model used here, as well as the LCC model, are based on experimental data from cardiac myocytes (Table 1) for which the kinetic constants are well studied. Three buffers were considered: (1) a fast, diffusible, high-affinity buffer, e.g. the fluorescent dye Fluo-4, (2) calmodulin (CaM) as an immobile, high-affinity buffer that mediates biologically relevant interactions, e.g. with protein kinases, and (3) the plasma membrane or sarcolemma (SL), a low-affinity buffer present at high concentrations (>1 μM).

Figure 4a shows the results of a representative simulation run in a $(0.5\ \mu\text{m})^3 = 0.125$ fl volume. The upper trace shows the reduced functional state of the LCC (closed-0, open-1). In all simulations, the channel only opened during the depolarisation step from −70 to +20 mV (25–75 ms). The middle trace shows the number of unbound $Ca^{2+}$ ions (on average ∼100 nM); in a single trace, the slightly

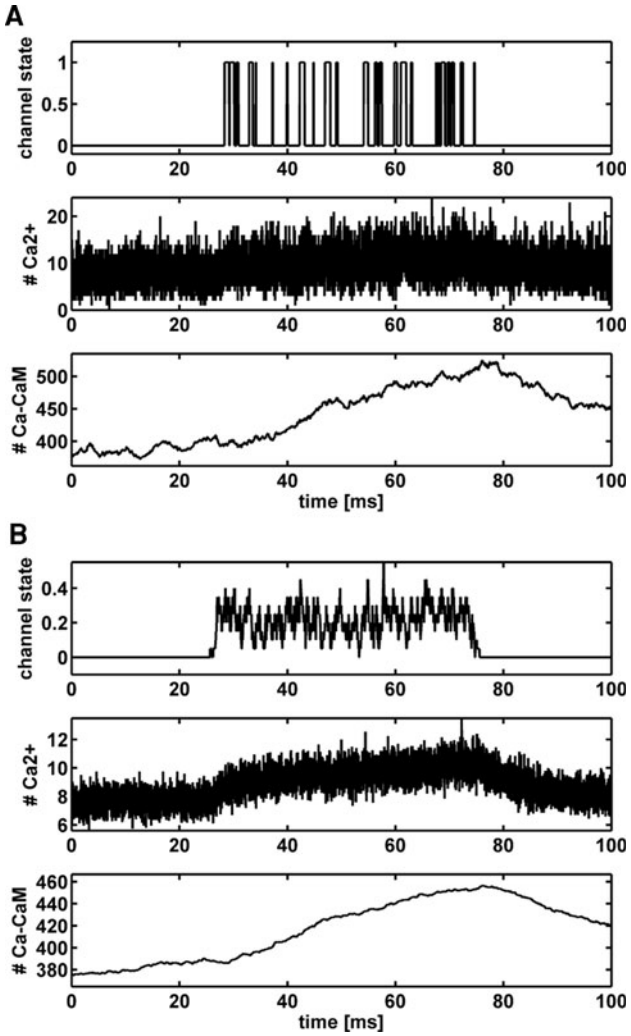


**Fig. 4** **a** Simulation of a single voxel with diffusion and LCC. LCC openings (*upper trace*, *0* closed, *1* open) only occur during the depolarisation step from −70 to +20 mV (25–75 ms). The number of $Ca^{2+}$ ions, shown in the middle trace, shows only a small increase, hardly visible by eye. The number of Ca–CaM complexes (*lower trace*) shows an increasing tendency during depolarisation and $Ca^{2+}$ release. **b** The effects are seen more clearly when the average of 20 runs is considered. In particular, the increased $Ca^{2+}$ concentration during depolarisation is now clearly distinguishable. The channel state has to be interpreted as the average open probability

increased $Ca^{2+}$ concentration due to channel openings is hardly visible, mainly because the mean LCC current at +20 mV is very low (approximately −0.05 pA, Jafri et al. 1998). The lower trace shows the number of Ca–CaM complexes present in the volume. This trace is shown as an indicator of the signal passed on to other subcellular signalling cascades. In signal processing terms, the Ca–CaM signal is approximately an integrated and low-pass filtered version of the $Ca^{2+}$ concentration. To illustrate the effects more clearly, Fig. 4b shows the average of 20 sample paths. Here, it is demonstrated that channel openings actually occur during membrane depolarisation and that the mean $Ca^{2+}$ concentration during this episode is significantly elevated. Upon close inspection, it is also seen that the $Ca^{2+}$ concentration in the microdomain keeps rising as long as channel openings occur. Similarly, the Ca–CaM signal shows a clear increase, although with a much lower variability, due to the high reactant count compared to $Ca^{2+}$. The variability of the Ca–CaM signal in shown in Fig. 5 where all 20 sample paths (grey curves) constituting the mean curve (black curve) are shown.

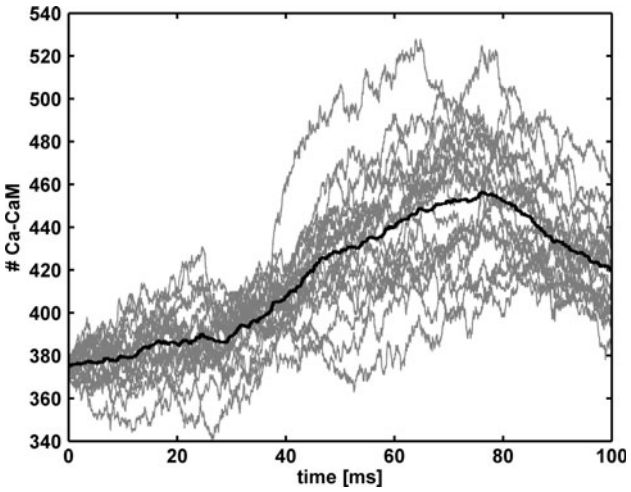


**Fig. 5** The number of calcium-bound CaM molecules (Ca–CaM) is shown for 20 simulation runs (*grey curves*). On average (*black curve*), the Ca–CaM count grows with a delay relative to the start of LCC openings. The mean response, approximating the deterministic limit, does not capture the considerable variability in individual responses, due to the intrinsic stochasticity of LCC openings, diffusion and $Ca^{2+}$ binding to CaM

### Computation time

Exemplary computaton times were 16 ± 3 s for a single simulation run as shown in Fig. 3b, i.e. the single-voxel algorithm with diffusion (1 fl, 100 ms) whereas a 100-ms simulation as shown in Fig. 3c (multivoxel) ran 6,709 ± 848 s ($n = 10$ for both cases). Another example: when the abundant $Ca^{2+}$-buffering membrane phospholipids for the reaction-diffusion system shown in Figs. 4 and 5 are assigned a positive diffusion constant of 25 $\mu m^2\ s^{-1}$, computation time increases from 48 ± 8 s (for an immobile buffer) to 292 ± 45 s ($n = 10$). These examples show that diffusion events mainly determine simulation time. In all systems discussed here, diffusion events outnumber chemical reaction events by a factor of at least 100.

## Discussion

In this report, we presented a stochastic simulation algorithm to study calcium microdomains in the vicinity of L-type calcium channels. The biological importance of these microdomains has been recognised in recent years, mainly due to crucial advances in experimental methods, e.g. laser microscopy techniques (Cheng and Lederer 2008). The term microdomain refers to sub-femtoliter volumes, a scale that also represents the resolution limit of state-of-the-art microscopes. Computational studies are frequently used to test theoretical models of subcellular processes and to design key experiments.

Most simulation studies of calcium microdomains include LCC, ryanodine receptor (RyR) and 1,4,5-inositol-trisphosphate receptor ($IP_3R$) $Ca^{2+}$ channels and use a hybrid simulation approach—the reaction-diffusion subsystem, in particular $Ca^{2+}$ buffering, is simulated in a deterministic way using discretised partial differential equations (PDE) whereas ion-channel gating is treated stochastically as a Markov process (Stern et al. 1997; Hinch et al. 2004; Greenstein and Winslow 2002; Rüdiger et al. 2007; Shuai et al. 2007; Shuai et al. 2008). A short calculation reveals that in a microdomain of $(0.5\ \mu m)^3$, only 7–8 $Ca^{2+}$ ions are present on average (given a resting equilibrium concentration of 100 nM $Ca^{2+}$). Moreover, the fusion of deterministic and stochastic processes in hybrid simulation schemes requires an extra effort and often involves approximation steps and/or computationally expensive 'quasi-infinitesimal' time increments.

For these reasons, our aim was to design a unified stochastic approach that implements all processes as a multivariate Markov process, possibly at a reasonable computational cost. The proposed solution is an extension of Gillespie's exact stochastic simulation algorithm (Gillespie 1977). To integrate $Ca^{2+}$ channels, the system needs a mechanism to relax to equilibrium when new $Ca^{2+}$ ions are introduced in the simulation volume. Therefore, diffusion, treated as a special kind of chemical reaction, is integrated as proposed by Elf (Elf et al. 2003). Further, to model voltage-dependency of the calcium channel, the continuously changing transition rate representing voltage-sensitive gating kinetics of the channel has to be included in the model. We show how random

waiting times for these steps can be simulated exactly and how the result fits into the Gillespie algorithm by simply extending the event waiting-time queue. Exact sampling of waiting-time distributions for continuously changing rates in the context of $Ca^{2+}$-channel modelling has also been used before (Mazzag et al. 2005; Rüdiger et al. 2007), with the latter based on an algorithm proposed by Alfonsi and colleagues (Alfonsi et al. 2005). These models, however, differ from the model developed here as they assume the calcium and buffer reaction-diffusion system as a deterministic process. Another purely stochastic model was proposed by Winslow and co-workers (Winslow et al. 2006), using a detailed model of the cardiac myocyte $Ca^{2+}$-release unit ('dyad'). From a theoretical point of view, their algorithm is based on the Fokker–Planck equation (a deterministic partial differential equation) describing the evolution of the probability density function of all molecules' spatial positions. The algorithm proposed here adopts the Langevin picture (Gillespie 2000), i.e. a stochastic ordinary differential equation, describing the dynamics of the number of reactants. When run with the same input parameters, i.e. the same model, both algorithms should provide equivalent results. An interesting topic of future investigations might be the comparison of both approaches with regard to computational efficiency.

In the future, even more details about channel function will have to be integrated in the model, e.g. channel inactivation and $Ca^{2+}$-dependent conductance, which were not evaluated in this study. On the other hand, we introduced conductance as a stochastic process, here, as a simple Poisson process. Experimental and modelling studies, however, give a more complex picture of ion permeation through protein nanopores and even suggest anomalous transport. Specific results for a given ion channel could be incorporated in the model we proposed in this work.

For the models used in this study, the single-voxel algorithm with diffusion proved to produce basically the same equilibrium statistics as the corresponding multivoxel simulation. The main advantage lies in the fact that computation time is reduced significantly and, thus, even relatively complex models can be run on a standard personal computer in a few minutes.

Most interestingly, the presented method may prove useful for 'in silico' investigations of stochastic effects, intrinsic to $Ca^{2+}$ microdomains, on downstream signalling cascades regulating cellular function. Viral infection can induce membrane depolarisation of the host cell, an effect that, in turn, can promote $Ca^{2+}$ influx into the host cell, e.g. via voltage-sensitive calcium channels. Membrane depolarisation has been shown to be directly mediated by viral ion-channel-forming proteins. A prominent example is given by the green alga Chlorella NC64A—when these cells are infected by PBCV-1 or NY-2A viruses, depolarisation is evoked by the viral Kcv channel, a $Cs^{+}$-sensitive $K^{+}$ channel (Frohns et al. 2006). Importantly, depolarisation appears to be a crucial event as shown by impaired virus replication after application of the Kcv-blocking agent $Cs^{+}$. Another biomedically relevant example is the HIV-1-encoded cation channel Vpr, which causes large inward currents in hippocampal neurons, a process assumed to be involved in AIDS-associated encephalopathy (Piller et al. 1998). As many viral channel-forming proteins preferentially conduct cations (Fischer and Sansom 2002), depolarisation is expected to occur in most cell types that incorporate these proteins in their membranes. It is also known that an increase in $[Ca^{2+}]$ is crucial for the subsequent processes involved in viral replication and virus release (Bouchard et al. 2001; Fischer and Sansom 2002). Combining biophysical data on newly discovered viral ion channels (Lu et al. 2006) with data on calcium homeostasis of host cells, the proposed method may help to elucidate mechanisms by which these pathogens interact with their environment.

## References


Alfonsi A, Cancès E, Turinici G, Di Ventura B, Huisinga W (2005) Adaptive simulation of hybrid stochastic and deterministic models for biochemical systems. ESAIM Proc 14:1–13

Bhalla U (2004) Signaling in small subcellular volumes. I. Stochastic diffusion effects on individual pathways. Biophys J 87:733–744

Bouchard MJ, Wang LH, Schneider RJ (2001) Calcium signaling by HBx protein in hepatitis B virus DNA replication. Science 294:2376–2378

Catterall W, Perez-Reyes E, Snutch TP, Striessnig J (2005) International Union of Pharmacology. XLVIII. Nomenclature and structure–function relationships of voltage-gated calcium channels. Pharmacol Rev 57:411–425

Cheng H, Lederer WJ (2008) Calcium sparks. Physiol Rev 88: 1491–1545

Demuro A, Parker I (2004) Imaging the activity and localization of single voltage-gated $Ca^{2+}$ channels by total internal reflection microscopy. Biophys J 86:3250–3259

Elf J, Doncic A, Ehrenberg M (2003) Mesoscopic reaction-diffusion in intracellular signaling. SPIE Proc 5110:114–125

Fischer WB (2005) Viral membrane proteins: structure, function and drug design, vol 1. Kluwer, New York

Fischer WB, Sansom MSP (2002) Viral ion channels: structure and function. Biochim Biophys Acta 1561:27–45

Frohns F, Käsmann A, Kramer D, Schäfer B, Mehmel M, Kang M, Van Etten JL, Gazzarrini S, Moroni A, Thiel G (2006) Potassium ion channels of chlorella viruses cause rapid depolarization of host cells during infection. J Virol 80(5):2437–2444

Gibson MA, Bruck J (2000) Efficient exact stochastic simulation of chemical systems with many species and many channels. J Phys Chem A 104:1876–1889

Gillespie DT (1977) Exact stochastic simulation of coupled chemical reactions. J Phys Chem 81(25):2340–2361

Gillespie DT (2000) The chemical Langevin equation. J Chem Phys 113(1):297–306

Greenstein JL, Winslow RL (2002) An integrative model of the cardiac ventricular myocyte incorporating local control of $Ca^{2+}$ release. Biophys J 83:2918–2945

Griffin SDC, Beales LP, Clarke DS, Worsfold O, Evans SD, Jaeger J, Harris MPG, Rowlands DJ (2003) The p7 protein of hepatitis C virus forms an ion channel that is blocked by the antiviral drug, amantadine. FEBS Lett 535:34–38

Hinch R, Greenstein JL, Tanskanen AJ, Xu L, Winslow RL (2004) A simplified local control model of calcium-induced calcium release in cardiac ventricular myocytes. Biophys J 87:3723–3736

Jafri MS, Rice JJ, Winslow RL (1998) Cardiac Ca2+ dynamics: the roles of ryanodine receptor adaptation and sarcoplasmic reticulum load. Biophys J 74:1149–1168

Jiang Y-H, Klein MG, Schneider MF (1999) Numerical simulation of $Ca^{2+}$ "sparks" in skeletal muscle. Biophys J 77:2333–2357

Keller DX, Franks KM, Bartol TM, Sejnowski TJ (2008) Calmodulin activation by calcium transients in the postsynaptic density of dendritic spines. PLoS ONE 3(4):e2045

Krishnamurty V, Chung SH (2007) Large scale dynamical models and estimation for permeation in biological membrane ion channels. Proc IEEE 95(5):853–880

Kuyucak S, Andersen OS, Chung SH (2001) Model of permeation in ion channels. Rep Prog Phys 64:1427–1472

Lu W, Zheng BJ, Xu K, Schwarz W, Du L, Wong CKL, Chen J, Duan S, Deubel V, Sun B (2006) Severe acute respiratory syndrome-associated coronavirus 3a protein forms an ion channel and modulates virus release. Proc Natl Acad Sci USA 103(33): 12540–12545

Mazzag B, Tignanelli CJ, Smith GD (2005) The effect of residual $Ca^{2+}$ on the stochastic gating of $Ca^{2+}$–regulated $Ca^{2+}$ channel models. J Theor Biol 235:121–150

Norris JR (1997) Markov chains. Cambridge University Press, London, pp 60–125

Piller SC, Jans P, Gage PW, Jans DA (1998) Extracellular HIV-1 virus protein R causes a large inward current and cell death in cultured hippocampal neurons: implications for AIDS patholgy. Proc Natl Acad Sci USA 95:4595–4600

Press WH, Teukolsky SA, Vetterling WT, Flannery BP (2002) Random numbers. Transformation method: exponential and normal deviates. In: Numerical recipes in C++, the art of scientific computing, 2nd edn. Cambridge University Press, London, pp 287–289

Rüdiger S, Shuai JW, Huisinga W, Nagaiah C, Warnecke G, Parker I, Falcke M (2007) Hybrid stochastic and deterministic simulations of calcium blips. Biophys J 93:1847–1857

Shuai JW, Pearson JE, Foskett JK, Mak DD, Parker I (2007) A kinetic model of single and clustered $IP_3$ receptors in the absence of $Ca^{2+}$ feedback. Biophys J 93:1151–1162

Shuai JW, Pearson JE, Parker I (2008) Modeling Ca2+ feedback on a single inositol 1,4,5-trisphosphate receptor and its modulation by Ca2+ buffers. Biophys J 95:3738–3752

Smith GD (2002) Modeling the stochastic gating of ion channels. In: Fall CP, Marland E, Wagner J, Tyson J (eds) Computational cell biology. Springer, Berlin, pp 289–296

Smith GD, Keizer JE, Stern MD, Lederer WJ, Cheng H (1998) A simple numerical model of calcium spark formation and detection in cardiac myocytes. Biophys J 75:15–32

Stern MD, Pizarro G, Ríos E (1997) Local control model excitation-contraction coupling in skeletal muscle. J Gen Physiol 110: 415–440

Stern MD, Song L-S, Cheng H, Sham JSK, Yang HT, Boheler KR, Ríos E (1999) Local control models of cardiac excitation–contraction coupling. A possible role for allosteric interactions between ryanodine receptors. J Gen Physiol 113:469–489

Uttenweiler D, Kirsch WG, Schulzke E, Both M, Fink RHA (2002) Model-based analysis of elementary $Ca^{2+}$ release events in skinned mammalian skeletal muscle fibres. Eur Biophys J 31:331–340

Winslow RL, Tanskanen A, Chen M, Greenstein JL (2006) Multiscale modeling of calcium signaling in the cardiac dyad. Ann NY Acad Sci 1080:362–375